In-pore tensile stress by drying-induced capillary bridges inside porous materials.

Majda Bouzid, Lionel Mercury, Arnault Lassin, Jean-Michel Matray, Mohamed Azaroual

IN-PORE TENSILE STRESS BY DRYING-INDUCED CAPILLARY BRIDGES INSIDE POROUS MATERIALS

Majda BOUZID[1,2], Lionel MERCURY[3,*], Arnault LASSIN[4], Jean-Michel MATRAY[2], Mohamed AZAROUAL[4]

[1] IDES, UMR 8148 CNRS/Université Paris-Sud, bâtiment 504, 91405 Orsay Cedex, France

[2] IRSN, DEI/SARG/LR2S, BP 17, 92262 Fontenay-aux-Roses Cedex, France

[3] Institut des Sciences de la Terre d'Orléans, UMR 6113 CNRS/Université d'Orléans, 1A rue de la Férolerie, 45071 Orléans Cedex, France.

[4] BRGM, Water Division, 3 av. C. Guillemin, 45060 Orléans Cedex 2, France

* Corresponding author: lionel.mercury@univ-orleans.fr. Tel: +33.(0)238.255.398; Fax: +33(0)238.636.488

Abstract.

We present here some evidences that capillary liquid bridges are able to deform micrometric cylindrical pores by tensile stress. Brine-soaked filter membranes are submitted to drying conditions leading to NaCl precipitation inside the 5-10 µm pores. A close examination demonstrated that two forms of NaCl crystallites are successively generated. First, primary cubic crystals grow, driven by the permanent evaporation. When this angular primary solid gets near the pore wall, while the evaporation makes the pore volume to be partly invaded by air, capillary liquid can bridge the now-small gap between the halite angles and the pore wall. In a second step, these small capillary bridges are frozen by a secondary precipitation event of concave-shaped NaCl. The proposed interpretation is that the liquid capillary bridges deform the host matrix of the membrane, and the situation is fossilized by the growth of solid capillary bridges. A quantitative interpretation is proposed and the consequences towards the natural media outlined.

Keywords: unsaturated zone, liquid water, tensile strength, poromechanics, soluble salts

1. INTRODUCTION

The porous or finely fractured unsaturated systems are widely present in natural systems, like the non-saturated soils or the three-phases oil-depleted aquifers, as well as in anthropogenized media like the excavation damaged zone around deep geological nuclear waste disposals. Another common such systems are the building stones when extracted from natural quarries, and exposed to drying-wetting cycles along an hydrological year. They typically contain water suspended over air against gravity, by bridging the solid-to-solid pore space owing to the capillary forces. The capillary state of the soil solutions has direct consequences on the mechanical equilibrium and the chemical weathering at the pore scale. The first effect is related to the time of the solid-aqueous solution interaction due to the immobilization of the capillary solutions (e.g., [1-2]). Another effect depends on the thermodynamic properties of a capillary liquid (and therefore its solvent properties) which differ from those of the free liquid [3-10]. On the mechanical side, capillary bridges pull on the solid(s) to which they are anchored, and so play a role in the compaction and the strength of soils (e.g., [11-13]), and in general of any granular wetted stacks (e.g., [14-15]). Furthermore, Scherer [16] and Smith et al. [17] for gels, Tas et al. [18,19] for massive solids (silicon chips), gave grounds that the capillary bridges are able to mechanically deform solid matrix, even at moderate capillary pressure.

In parallel, many field observations in the arid zones report the erosive role of the salts precipitating in the micro-porous regions of rocks, due to the drying of the network. Salt weathering is able to provoke the *in situ* breakdown of massive rocks like granite (e.g., [20-24]). That corresponds to coupled processes, interlinking chemistry and mechanics taking into account the capillary state of the media. The Wellman and Wilson's model highlighted the role of the smaller pores and the salt precipitation inside them to provoke the most efficient rock breakdown in coastal and arid environments. Scherer [16] highlighted the role of the small pores by replacing the discussion in the context of the drying of any heterometric pore network: as the large pores empty first, then the tension in the neighbouring small pores

may deform the pore wall and causes cracking (see especially the Fig. 7 in [16]). Meanwhile, a lot of parameters are acting in these processes, as the host microstructural properties, the environmental conditions, the interfacial tensions, or still the composition of the soaking solution, and so the causal connections are very complex to decompose.

The present paper reports simple experiments targeting to illustrate how the capillarity may take place in the salt weathering process. To do that, we decided to work with hand-made saline solutions, (initially) saturating homogeneous simple pores under soft drying conditions. After detailing the protocol and the main results, we will present a thermodynamic interpretation of the successive events which includes the capillarity arising during the drying. Clues of the occurrence of this capillary weathering in the fields are collected to outline the potential importance of this effect in non-saturated media, submitted to drying-wetting cycles, typically natural soils or the area around any excavated tunnels. However, the complexity of such media makes this endeavour very exploratory, and worth to be deepened in the future by field geochemists.

2. BACK TO CAPILLARITY

The conditions of occurrence of capillarity have been treated for long with the respective roles of the pore radius (Young-Laplace law) and of the Relative Humidity (RH hereafter) of air (Kelvin law) inside the system.

2.1 Young-Laplace law

The first capillarity “Young-Laplace” law correlates the curvature of an interface with the pressure difference across it. For a liquid-air interface:

$$\Delta P = \gamma_{LV} \times \left(\frac{1}{r_1} + \frac{1}{r_2} \right) \tag{1a}$$

with $\Delta P = P_L - P_V$ is the pressure difference (in Pa) between the liquid phase (at P_L) and the air phase (at P_V). As capillary menisci are concave towards the atmosphere, the liquid pressure is lower than that of the atmosphere, possibly reaching negative values (commonly

called tensile or stretched liquid water) while vapour pressure is obviously always positive. r_1 and r_2 (in meters), are the main radii of curvature of the meniscus, and for spherical meniscus: $r_1 = r_2$. The radius is counted negative for concave meniscus (positive for a droplet), which maintains the correct sign balance between the two members of equation (1). γ_{LV} is the surface tension between the liquid water and the vapour in air, and its high value for H_2O at room temperature is one of the reasons allowing the liquid water to to undergo high curvatures.

2.2 Capillary-elastic pressure for solids

The Young-Laplace law also applies to the solid-air interface and writes for a spherical interface:

$$\Delta P = \gamma_{SV} \times \left(\frac{1}{r_1} + \frac{1}{r_2} \right) \quad (1b)$$

with $\Delta P = P_S - P_V$ is the pressure difference (in Pa) between the solid phase (at P_V) and the air (at P_V); γ_{SV} is the surface tension between the air and the solid having a concave spherical curvature toward the air defined by r_1 and r_2.

One possible ambiguity comes from the twofold origin of the “solid pressure” parameter. Actually, it can be related to both an energy concept (chemical free energy of the solid) and a mechanical concept (surface stress). Cahn [25] outlined that the solid surfaces can change either by creating or destroying surface at constant surface structure and properties, or by an elastic strain along the surface at constant number of surface lattice sites. The first case requires a chemical driving force correlated to the surface free energy (work of creating a unit area of surface), the second requires a mechanical driving force correlated to the surface stress (work of elastic deformation of the surface). When one applies principles of capillarity to solids, the pressure jump across the interface and the corresponding shape of the interface obviously refer to a Gibbs free energy effect. It is why the capillary pressure jump is sometimes called the capillary-elastic pressure (e.g., [26]).

The chemical potentials of the naturally shaped solids are tabulated so that to meet the known solubility (in aqueous solutions) at normal conditions. In this sense, these chemical potentials are the 10^5 Pa reference. Any perturbation of the system pressure makes the chemical potential to vary by the V_s.dP term, V_s being the (assumed) constant solid volume. It follows that the Young-Laplace law applied to a solid-air equilibrium can be rewritten as:

$$\Delta P = \frac{\Delta \mu_S}{V_S} = \gamma_{SV} \times \left(\frac{1}{r_1} + \frac{1}{r_2} \right) \quad (1c)$$

Where $\Delta\mu_S = \mu_{solid,1bar} - \mu_{capillary\ solid}$ is the difference in the chemical potentials between the two forms of the given mineral. Equation (1c) correlates the shape change of a solid as a function of the capillary state inside the studied system to a solid pressure variation through the usual surface tension parameter.

2.3 Kelvin law

The second capillarity “Kelvin” law makes clear that the driving force to “capillarize” is the difference between the chemical potentials of the two partners separated by the curved interface. Again, for one liquid-air interface, that writes:

$$\log \frac{p}{p^\circ} = \frac{\Delta P . V_L}{RT \ln 10} \quad (2)$$

where p and $p°$, in Pa, are the pressure in equilibrium with, respectively, the curved and the plane interface; V_L, in m^3/mol, is the molar volume of the liquid, stated constant as a function of P_L; ΔP is the Young-Laplace pressure difference across the interface (equation 1a).

3. PROTOCOL AND EXPERIMENTAL TECHNIQUES

Polycarbonates membranes (filters) having homogeneous pores, in size (10 and 5 µm) and shape (cylindrical), are soaked with brines in a Petri cell filled with the suitable solution (see below). After, they are put in a drying chamber under fixed relative humidity (RH hereafter) of air, set to favor the water evaporation which should lead to the precipitation of solid salts

inside the initially large and cylindrical pores. After 15-20 days, the remaining brine is removed and the filters are directly observed by scanning electron microscopy (SEM).

3.1 Filters

The basic materials are polycarbonate membranes (Nuclepore, Whatman), whose pores are drilled by laser resulting in a perfect round shape (Fig. 1).

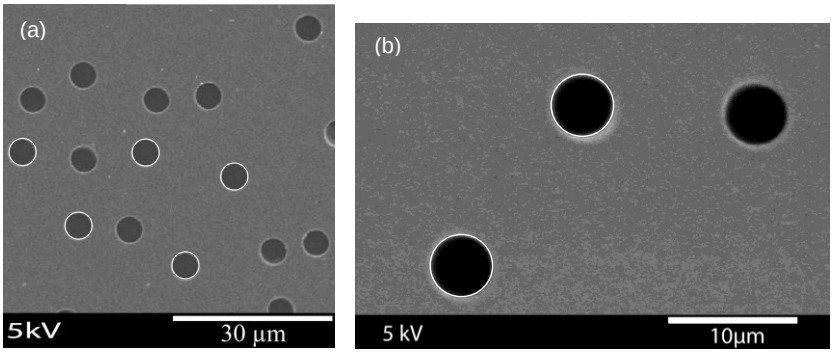

Figure 1. (a). Micrograph of a pristine membrane. Note the roundness and the regularity of the pores (highlighted by a white circle of the exact scaled size). (b) Micrograph of a membrane processed with pure water: pores after drying are always perfectly round.

The reproducibility of the drilled shape is very good as exemplified by the white circles, all of the expected scaled size. The pores are scattered on the whole surface (membrane diameter: 47 mm), and the depth of each pore equals the thickness of the membrane, around 10 microns. The membranes are made of polyaliphatic carbonates and so are totally non-hygroscopic, especially toward the atmospheric moisture. To test the stability of the pore geometry throughout the drying process, irrespective of other geochemical event, we compared the before-after states with one membrane soaked in pure water (Fig. 1b). It becomes obvious that the pristine membrane (Fig. 1a) and the water-treated one (Fig. 1b) are identical, establishing that the protocol, especially the drying stage (see below), is not able to modify the pore geometry. That is consistent with the hydrophobic behaviour of the polycarbonate itself.

3.2 Salt solution and solid salt

The sodium chloride (NaCl) is commonly encountered in salt crystallization decay and is frequently used for salt crystallisation laboratory tests (e.g., [27-28]). A vast literature deals with what happens when saline solutions evaporate in pores, and the subsequent phase transitions (e.g., [29-33]). This background gives us a large amount of very useful observations and measurements, but also relevant ideas on protocols and experimental methods.

Under room conditions, the sodium chloride–water system has one stable phase: halite (NaCl). The aqueous solutions are hand-made (NormaPur powder, Prolabo; milli-Q water) close to saturation: concentration is 5.5 mol/kg, at equilibrium with a 77% RH of air and slightly undersaturated with respect to halite (saturation is at 6.2 mol/kg at 25°C and 0.1 MPa).

3.3 Experimental procedure

The filters are individually soaked in the experimental solution, and then stacked upon each other (about ten) in a cylindrical container having the same 47 mm diameter as the filters. The container contains only the wetted filters (no free solution inside) and is put in a dry chamber where RH (75%) and temperature (20°C) are controlled. The RH is maintained constant by a saturated solution of NaCl put at the bottom of the dry chamber, and is recorded with a humidity/temperature data logger (EL-USB-2, LASCAR-Easylog): it never changed outside the ± 5% precision along all the experiments. The saturated bottom solution maintains slightly dry conditions inside the chamber, with respect to the (slightly) undersaturated solution trapped inside the filters (75% against 77%). By that way, we ensured a moderate evaporation, propitious to let the system adjust to geochemical and/or mechanical changes.

After 20 days in the dry chamber, the membrane located in the middle of the “membranes cake” is sampled and rinsed by vacuum filtration with water-repellent solvent (cyclohexane). The apolar solvent is poured onto the filter and is drawn throughout into a flask below by a

vacuum. The filtration time was shorter than one minute, and the applied vacuum was a classic primary vacuum with the residual gas pressure (in the flask) around $15x10^2$ Pa (around 98% vacuum). By that rinsing, we searched to fossilize the situation inside pores at the dry chamber state, extracting the aqueous solution remaining at this time. After, the rinsed membranes were gold/palladium-coated to enable the filter be observed with high vacuum SEM. By that way, we targeted to directly see what happened in the pores during the drying, which have been fossilized by the preparation procedure. These observations were performed at the IRSN laboratory of Fontenay-aux-Roses with a HITACHI S-3500 N.

3.4 *in situ* observation

The vacuum conditions of the SEM stage may cast doubt that the secondary solids precipitated in pores are really associated with the drying conditions of the chamber and not with the experimental procedure (especially the SEM stage). The problem is to warrant that the rinsing procedure actually expels the water retained in pores. Due to the importance to avoid any artefact, we also made some cross observations with an environmental scanning electron microscope (ESEM, FEI Quanta 200F) at the School of Mines of Ales (France). The sample was taken in the drying chamber and directly put in the microscope (neither filtration, nor metallization, nor any vacuum), set up to the same (T, RH) conditions as those existing in the drying chamber (75%, 20°C).

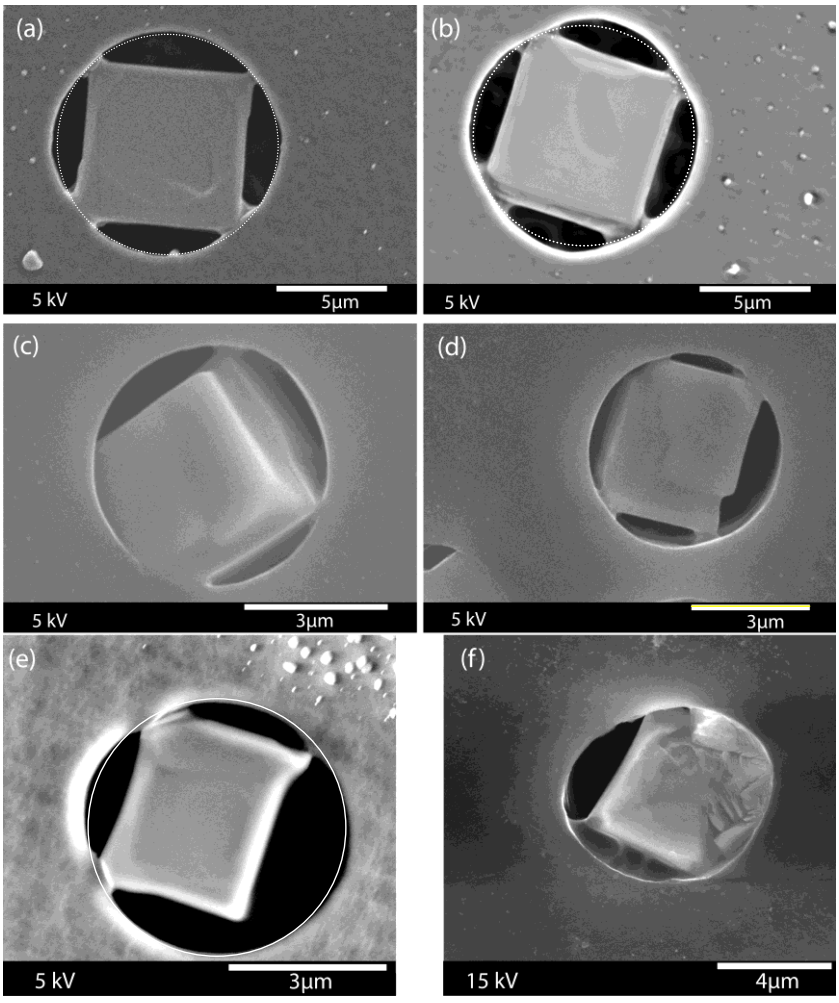

Figure 2. NaCl having grown in pores during 20 days at 75% RH (73 ± 2% RH for 2f) and 20°C, as displayed by SEM (a-d) and ESEM (e-f). (a-b) pore diameter = 10 µm; (c-f) pore diameter = 5 µm. Two generations of NaCl are visible: a primary cubic massive crystal and an often-curved secondary one.

The SEM (Figs 2a-d) and ESEM (Figs 2e-f) pictures show the same main features: one crystal grown in the pore, and able to deform the membrane when it interacts with it. This similarity gives ground that the cyclohexane rinsing effectively expelled the pore brine. As the quality of the observation is better with the SEM micrographs at a much lower cost, almost all pictures were recorded with SEM. Actually, the ESEM experiences were not able to keep stable conditions, and after around 10 minutes, systematically showed strong deformations of all the pores membranes, irrespective of any salt precipitation but due to drier conditions than those set on. That prevented us to directly observe the whole process described below.

4. RESULTS

Under the drying conditions, the brine filling the pores of the membrane concentrates so that NaCl can precipitate in pores. A cubic (natural shape) crystal develops in the centre of the pore, and, very often (not to say always), develops NaCl-membrane interactions at those corners that are close to the membrane (Fig. 2). According to Sunagawa [34], the cubic shape is characteristic of a NaCl growth at low supersaturation, in quasi-equilibrium with the solution. That means, as expected, the drying process does not proceed violently thanks to the low RH gradient, and allows the cubic NaCl to grow in the whole volume (see especially Figs 2c,d). In addition to this highly reproducible habit, two observations are worth to be noticed on the micrographs.

- An ellipsoidal deformation of the global pore, visually in line with the touching corner(s) of the grown NaCl. The deformation clearly corresponds to a pulling effect from around the touching corners;
- At these touching corners where the deformation is maximal, we observe (more or less developed/visible) NaCl precipitates with a concave curvature toward the air.

4.1 Membrane deformation

The first observation, though surprising, is checked in every membrane, and establishes the fact of the in-pore traction. We hypothesize that this traction emanates from the liquid capillary bridges, taking place at the halite-pore contact during the drying process (see fig. 2f). This initial liquid traction is relayed by the solid traction when the capillary bridges turn to be solid, and so the deformation is maintained in the pore. Additionally, the sample displayed on figures 2a and b has been rinsed with pure water, two years after the initial soaking stage, and observed again (Fig. 3). It appears clearly that the membrane keeps its deformation, approximately at the same intensity (strain around 3% in the vertical plane of the figure 3a, for instance). This observation points to a (at least partly) irreversible behaviour during the deformation though the micro-mechanisms involved are unknown.

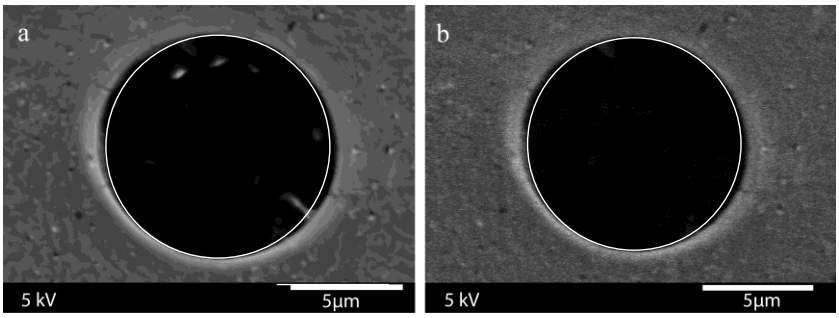

Figure 3. Two pores of the 10 µm membrane of figure 2, once the precipitated salts were removed by dilution. The membrane keeps deformed and seems micro-cracked, demonstrating the potential geomechanical power of the in-pore capillary traction.

Furthermore, the figures 3a and 3b shows a sort of halo all around the pore, approximately 0,7 µm width, with seemingly micro-cracking located at the previous most deformed places (see especially the top left quadrant). A similar halo of the same size is visible on the figure 3b (see also a micro-crack in the bottom right quadrant), though less clearly. These observations would tend to indicate that the deformation propagates inside the membrane and starts disrupting the cohesion of the polycarbonate polymer. This conclusion remains surprising because the tensile strength of the polycarbonate polymers ranges over 550-750x10^5 Pa (see below the values of capillary pressure, around 10x10^5 Pa) and that an elongation of at least 80% (instead of our 3%) is required to break the material ("polycarbonate" item in Wikipedia). We hypothesize that the duration of the traction (two years), though weak, should have led to these first micro-cracks. Also, as the deformation is located on tiny contacts, it is possible that the corresponding local elongation reaches high values.

To go further, the deformation can be measured directly on the micrographs and the corresponding traction thus evaluated. With the figure 2a, taken the distances at the equatorial plane of the circle, we measure an ellipsoidal elongation of maximum 0.33 µm (over 10 µm diameter), saying a 3% variation. For the sake of comparison, Tas et al. [18] measured a 7.5% deflection in the centre of rectangular 100 nm channels, filled with capillary water.

This deformation only affects the membrane, while the cubic halite remains straight. This differential behaviour can be accounted for by comparing the Young's modulus of the two solids: 2.2×10^9 Pa for polycarbonates (e.g. "polycarbonate" item in Wikipedia), and at least 20×10^9 Pa for the halite (as an ionic solid).

Tas et al [18] measured a 7.5 nm deflection of their 0.8 µm capping silicon layer ($E = 70 \times 10^9$ Pa), which requires a water pressure of -17×10^5 Pa ± 10 assuming a total transmission of the capillary forces to the solid (no adhesion effect, [19]). The polycarbonate is 30 times softer than the silicon, and the length variations is 2.5 times smaller in the polycarbonate experiments: at constant geometry, we should expect that the capillary pressure in our experiment is 12 times weaker than that in the nanochannels experiment, namely roughly -1.5×10^5 Pa. This last value certainly underestimates the real one due to the difference in the geometries of the pulling bridges. We can safely pretend that the right value should range between this low value up to an upper limit, saying one order of magnitude higher (-15×10^5 Pa).

4.2 NaCl capillary bridges

The second surprising observation is the occurrence of curved NaCl in contact with the primary massive cubic NaCl. The 2a,b figures, taken in the same 10 µm membranes, are the most impressive displaying very clearly capillary bridges at the contacting NaCl corners. As these are SEM micrographs, the capillary bridges are forcibly NaCl-made and have approximately the same curvature, 0.7±0.1 µm. The uncertainty is pretty large since it is difficult to be sure that we really observe the very contact between the two sides of the bridges. Also, the figures 2c,d (5 µm diameter pores) display less visible (NaCl) capillary bridges, associated with a less pronounced deformation: approximately 0.09 µm on a 5 µm diameter (1.8% variation), that is to say twice less than the deformation displayed on figures 2a,b. Therefore, it appears that the global deformation of the pore depends on the size of the bridge as well as the intensity of its internal traction.

The curvature of the NaCl bridges can serve to evaluate the capillary pressure existing inside the capillarized solid. We write:

$$r_1 = \frac{h}{2\cos(\alpha + \theta)} \tag{3}$$

where θ is the contact angle between the solution and the pore wall or NaCl crystal, and α the angle between the cubic halite and the pore wall at the junction point (Fig. 4b). The two main radius of curvature of the capillary meniscus (see equation (1)) simplifies, because r_2 is largely higher than r_1. A simple geometrical relationship (Figs 4c,d) relates the r_1 in the xy-plane to the distance separating the two solids *h*, while the r_2 is related to the length pore *e*. As the *e* distance is quite larger than the *h* distance (Fig. 4d), and with the absence of perpendicular solids on the yz-plane, the $1/r_2$ term can be neglected.

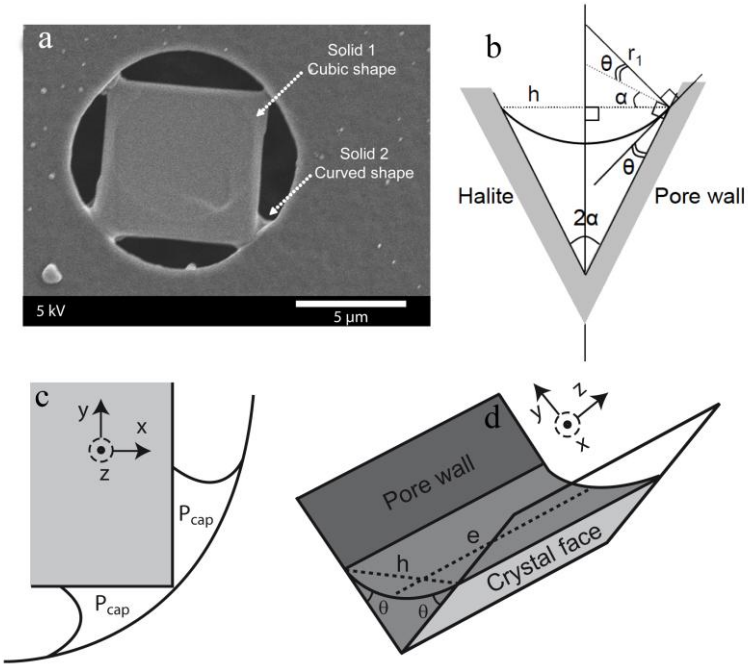

Figure 4. (a) NaCl SEM micrograph showing the massive form ("solid 1") precipitated from bulk evaporating solution and the curved form ("solid 2") which records the capillary conditions of the mother solution. (b) Geometrical Young-Laplace parameters according to the NaCl-pore wall contact. (c) Sketch showing the capillarized solution trapped between the NaCl primary crystal and pore membrane wall, before the secondary precipitation. (d) Meniscus curvature between the two solids (NaCl crystals and pore wall) in the yz-plane.

Combining equations (1) and (3) gives the pressure drop across the solid meniscus:

$$\Delta P_{cap} = P_{atm} - P_{CapillaryBridge} = \frac{2\gamma_{SV}\cos(\alpha+\theta)}{h} \quad (4)$$

Based on measurements from the micrographs 2a,b, the distance *h* between the two solids was estimated to 0.7±0.1 µm, the contact angle θ between the pore wall and the bridge is put to 0° because the real halite-membrane contact is not precisely visible, and the α angle is measured to around 21°. The γ_{SV} term is the NaCl-air surface tension, equal to 200 mJ.m^{-2} [35]. With these values, equation (4) predicts a pressure drop of 5x10^5 Pa. For an ambient atmospheric pressure (P_{atm} = 10^5 Pa), the capillary pressure existing in the curved solid is therefore around -4x10^5 Pa, which is close to the previous estimate (-1.5x10^5 Pa).

4.3 Size effect and bridge traction

The above micrographs constitute firm grounds that capillary bridges of the mother solution existed at the NaCl-membrane corners during the drying and were replaced later by solid capillary bridges. Otherwise speaking, the aqueous solution filling the wedge formed between the cubic corner and the pore membrane first capillarizes significantly, owing to the small distance from one solid to the other (*h* parameter in equation 4). It is clear that the distance between the NaCl corner and the pore must be reduced sufficiently for a capillary liquid bridge to form, prior to the precipitation of the secondary curved NaCl. The free corner on figure 2e (bottom right) exemplifies this point: the corner-wall distance is too large and prevents a capillary liquid bridge (and therefore a secondary curved solid) from taking place. The figure 2e displays a regular shape in the bottom right quadrant which leads us to another conclusion: whenever the precipitated salt and the pore wall are not bridged, no deformation occurs on the corresponding section of the surrounding solid, except that depending on the three anchorage points. This seems a firm fact (in our opinion) that the observed strain is controlled by the bridges.

A last observation is worth to be outlined about the tri-dimensional shape of the capillary bridges. A careful examination of the 2c and 2d micrographs lets to think that the capillary

bridges extend inside the depth of the pore, especially when examining the bridges at the top right corners on the micrographs. The bridges seem to extend in a more or less cylindrical manner, indicating that the capillary bridge effect is not related to the position at the outer extremity of the pore, but is a “volume” effect.

5. INTERPRETATION

5.1 Primary in-pore halite

As the evaporation progresses, the solution is receding inside the pore, and concentration of dissolved species is increasing up to a stabilized value corresponding to equilibrium (or close) with the naturally-shaped (cubic) halite. The corresponding reaction writes:

$$Na^{+}_{(AQUEOUS)} + Cl^{-}_{(AQUEOUS)} \leftrightarrows NaCl_{(SOLID)} \quad (5)$$

The advancement of this reaction depends on the ratio between the equilibrium constant at the standard state (K) and the actual composition and activities of the dissolved solutes (ionic activity product, Q). The driving force for the precipitation of the primary massive NaCl is supplied by the evaporation which pulls the Q value above the K one, so that precipitation can occur according to the mass action law. Additionally, the present cubic habit indicates a precipitation at low supersaturation, close to equilibrium [34].

When the amount of solution becomes short with respect to the pore volume, and if the cube of NaCl is sufficiently close to the pore wall, the remaining solution can capillarilly bridge the pore space between the NaCl and the membrane (see §4.3). In this configuration, the system is more or less at equilibrium with respect to the local (at the pore scale) RH in air (Kelvin condition, see equation 2), and so the curved liquid ceases (or close) to evaporate, and then to concentrate. Meanwhile, the concentration in the capillary solution is most probably at equilibrium with the primary NaCl, due to the large surface to volume ratio between the tiny capillary bridge and the relatively large NaCl-solution contacting surface. But what is the solubility of the primary halite in a capillary solution?

Thermodynamically, the solid in its recognized natural shape is stated at 10^5 Pa, so that its chemical potential is correctly described by the reference Gibbs free energy (see §2.3). However, a change of the equilibrium constant happens due to the change in the thermochemical state of the liquid, which writes:

$$d\Delta_R G_{cap} = \int_{P_{ref}=0.1}^{P} -(V_{Na^+} + V_{Cl^-})dP = RT \ln \frac{K^\circ}{K_{anisobaric}} \quad (6)$$

where R is the ideal gases constant (in J.mol^{-1}.K^{-1}), T the temperature (in K), $d\Delta_R G_{cap}$ (in J.mol^{-1}) the change of the Gibbs free energy due to the capillarization inside the system, V_i (in m^3.mol^{-1}) the molar volume of the ith species, P (in Pa) the liquid phase pressure; $K_{anisobaric}$ and K° are the equilibrium constants of the halite precipitation reaction at P and 10^5 Pa, respectively. Such calculations with the equilibrium constants relate to an activity ratio, therefore without correction on the activity coefficients.

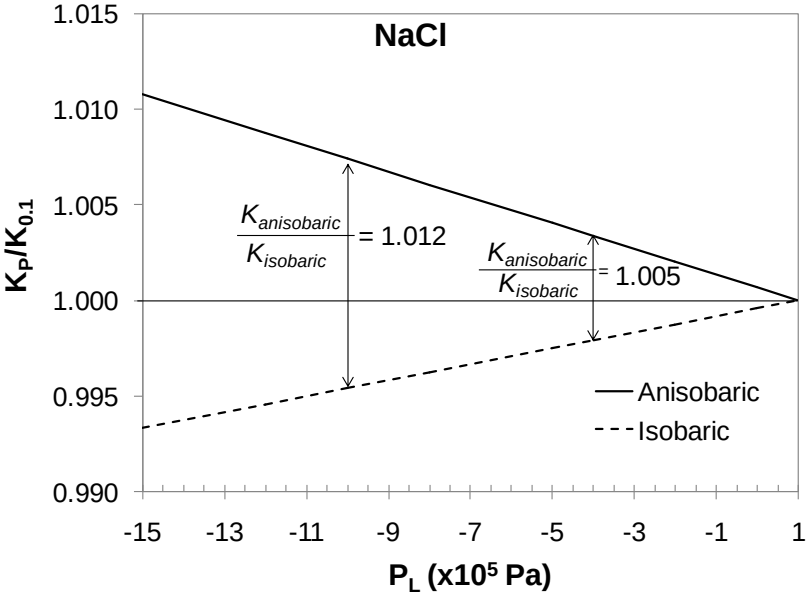

Figure 5. K_P/K° ratio for NaCl precipitation as a function of capillary pressure, according to the isobaric and anisobaric contexts (see text; thermodynamic properties from the Thermoddem database, available at http://thermoddem. brgm.fr/).

This configuration is called anisobaric (e.g., [8,10]) ("$K_{anisobaric}$"), since the cubic solid and the capillary solution do not experience the same pressure. The corresponding phase diagram is drawn on figure 5 using the THERMO-ZNS computer code, built for thermodynamic

calculations in capillary contexts (e.g., [10]). It shows that the corresponding $K_{anisobaric}$ increases with decreasing P, meaning that the halite is more soluble in capillary solution than in a free solution. In other words, bulk solution at equilibrium with cubic halite tends to become dissolving when it is capillarized. As a consequence, the chemical driving force in the system is toward the dissolution of the primary in-pore halite. Figure 5 shows that the capillarization of the liquid is probably accompanied by a solute enrichment in the solution, which is calculated with the Pitzer correction [36] on the figure 6. The upward arrow makes clear that a capillary solution has an increasing equilibrium constant, meaning that, under capillary conditions, the solution dissolves the naturally-shaped solid more than a free solution does. The downward arrow exemplifies the proposed driving force to build capillary solids (see below): when the ratio between the anisobaric and the isobaric situation increases enough, this supersaturation affords the required chemical energy for an isobaric (then curved) solid to grow.

5.2 Secondary in-pore halite

The second stage is the precipitation of the curved NaCl, corresponding to a different pattern than the easiest (low-cost) epitaxial growth on the pre-existing NaCl surface. There is a new process associated with a concave curvature, namely integrating the new capillary conditions of the mother solution. Thermodynamically, if the solid is impacted by the same capillary conditions as the solution, equation (6) becomes:

$$d\Delta_R G_{cap} = \int_{0.1}^{P} V_{NaCl_{cristal}}\, dP - \int_{0.1}^{P} (V_{Na^+} + V_{Cl^-})\, dP = RT \ln \frac{K^\circ}{K_{isobaric}} \qquad (7)$$

with V_{NaCl} (in $m^3.mol^{-1}$) the molar volume of the capillary crystal growing from the capillary solution, P (in Pa) the liquid or solid phase pressure; $K_{isobaric}$ and $K°$ are the equilibrium constants of the halite precipitation reaction at P and 10^5 Pa, respectively.

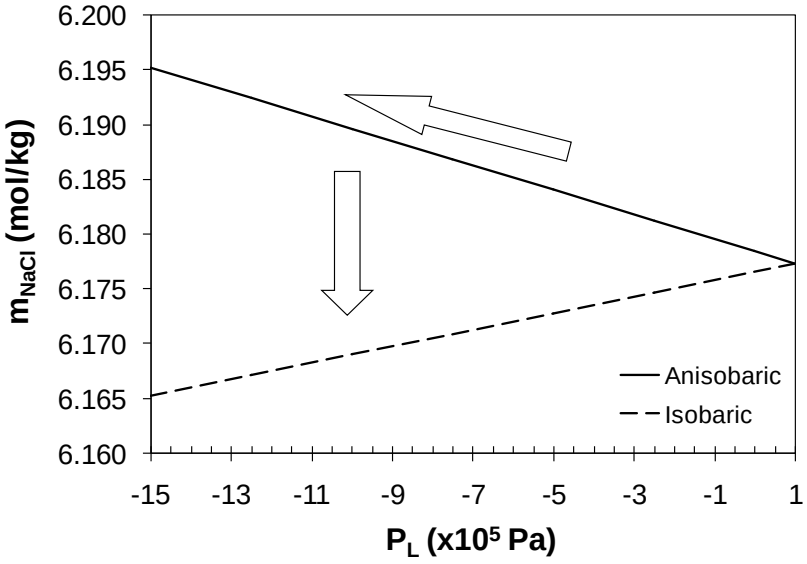

Figure 6. NaCl molality in the capillary brine at equilibrium with the cubic (anisobaric) and curved (isobaric) solids.

In the isobaric case ($P = P_{liquid} = P_{solid}$), the NaCl crystal is growing at the same pressure than the solution, which means it grows with a concave curvature more or less similar to that of the liquid. Precisely, if the capillary pressures of the solution and the solid are the same, the liquid-air and solid-air curvatures will be different by the difference in the γ terms (equation 1), between γ_{LV} (82 mJ.m^{-2} for a saturated NaCl solution, [37]) and γ_{SV} (200 mJ.m^{-2}, [35]).

The corresponding $K_{isobaric}$ is lower than $K°$, and then much lower than is $K_{anisobaric}$ (Fig. 5). Even if the capillary solution kept the same composition as the initial bulk one, it is now supersaturated with respect to the curved solid. And if the capillary solution starts dissolving the naturally-shaped solid according to the anisobaric scenario (which is the most probable), then the supersaturation increases. Therefore, there is a driving force now in the system toward the precipitation of an isobaric NaCl solid phase, owing to the capillarization of the solution and a possible re-dissolution of the primary solid. But this precipitation must occur through a special shape, characteristic of the capillary state of the solid (isobaric configuration).

Obviously, the ratio at -4.10^5 Pa (our capillary pressure) is pretty modest (see y axis in Fig. 5): $K_{anisobaric}/K_{isobaric}$ = 1.005, amounting to an excess of 14 J/mol of the Gibbs free energy of

the precipitation. At -15x10^5 Pa, $K_{anisobaric}/K_{isobaric}$ = 1.018 corresponding to an excess of 43 J/mol. These low excesses of chemical potential are explicitly assumed to supply the required energy to resume the precipitation and change the habit of the precipitate.

In general, the relationship between the crystal habits and the local physico-chemical conditions are well-known. The ice habit, for instance, can be predicted as a function of the solidification temperature. More generally, the building of small-size crystals requires more chemical energy than the large-size ones, and this excess is supplied by the supersaturation of the solution (Ostwald-Freundlich equation). In the present experiment, an excess amount of chemical energy is made available by the change of the equilibrium constant due to the building of capillary conditions. We propose that this is the driving force for the “freezing” of capillarity by the newly-grown concave crystal.

These concave crystals can be related to the hopper-shaped crystals, generally interpreted by a differential growth rate between the middle and the corners and edges of a face (e.g., [38]). Meanwhile, in concretion-forming (pore-space controlled) processes, they are known to precipitate in a second stage of the concretionary growth, after the first pore-filling stage [38]. Aside the diffusion-controlled growth already proposed [38], we may outline that the hopper shape is consistent with a capillarity-controlled precipitation.

6. FIELD-SCALE PERSPECTIVES

The arguments detailed along the previous sections led us to conclude that we have identified in this cylindrical 10 µm polycarbonate pore, the same phenomenon as Tas et al [18] did in their rectangular 100 nm silicon channels: the occurrence of capillary traction inside water unsaturated pores. But two new points are worth to be outlined: 1/ the traction occurs in a micrometric cylindrical pores, *a priori* unfavorable to such occurrence, owing to a prior precipitation event which greatly changes the topology of the pore space; 2/ the traction by liquid capillary bridges (Tas et al’s case) is fossilized by the precipitation of a capillarized

solid, which seems able to provoke micro-cracking in the solid (Fig. 3), probably linked to the duration of the traction event, and the irreversible path of the deformation.

Therefore, capillary bridging should contribute to the global strain inside a non-saturated object/system, as already stated for shrinkage and cracking in sol-gel drying processes [16-17]. Moreover, the in-pore mechanical traction exerted by the liquid capillary bridges can be relayed by solid capillary bridges which install the traction on a longer scale. These facts indicate that our experiments are of value to study the coupling between the local phase transitions and the poro-mechanics inside porous samples (membrane technologies largely used for the desalination processes for instance; salt damage in building stones; soil mechanics).

One field situation presents clues of the occurrence of the in-pore capillary traction. Inside the excavation damaged zone around drifts excavated in mines, tunnels or in underground research laboratories, several kinds of disturbances change the initial hydrogeological, geochemical and rock mechanical properties. Amongst these disturbances, it is commonly noticed the occurrence of an unsaturated zone with a wide variation of the pore sizes and degree of saturation. Very often, seasonal micro-cracks were observed *in situ*, which are often (and surprisingly) secant to the bedding [39]. Also, the cracks open during the cold and dry winter and close on hot and wet summer, which is the expected behavior, but during some slightly less wet seasons, the closing is not complete [40]. Meanwhile, the chemical analyses have proven that resident solutions can be concentrated up to gypsum precipitation [41]. Moreover, and this is the most significant in our opinion, gypsum precipitates are always associated with the largest cracks [41]. This is generally explained by the first formation of the cracking, which subsequently promotes the evaporation of the resident solution up to the precipitation threshold. But this explanation accounts neither for the secant cracking, nor for the irreversibility of the aperture. Our work paves the way for another explanation based on the occurrence of the two stages of the in-pore capillary traction, above detailed. Just to illustrate, we can mention that gypsum behaves the same way as the halite when drawn along the same thermodynamic cycle (Fig. 7).

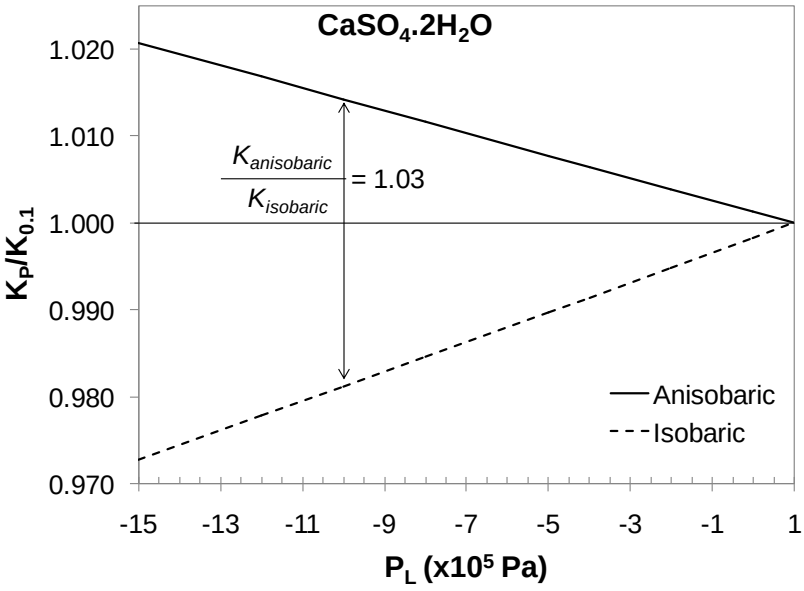

Figure 7. $K_P/K°$ ratio for $CaSO_4.2H_2O$ precipitation as a function of capillary pressure, through isobaric and anisobaric contexts (see text; thermodynamic properties from the Thermoddem database, available at http://thermoddem.brgm.fr/).

7. CONCLUSION

The experiments proposed in this paper are very simple and focused on getting a direct answer to the following question: what are the consequences of a drying desaturation process acting in an initially-saturated porous medium? We chose to carry out experiments in model materials having large cylindrical pores to make the observations easy and the chain of events simple and straightforward.

These experiments led us to get two different NaCl habits, coexisting in the same pore submitted to constant drying conditions. We observed first a primary massive precipitate having the cubic shape of NaCl. This habit is linked to a precipitation from a bulk solution supersaturated by evaporation due to the drying conditions. The secondary curved NaCl is interpreted as a precipitation inside a capillary aqueous solution and controlled by it, under a driving force generated by the change of the equilibrium constant K. The corresponding calculations have been accounted for by the isobaric-anisobaric frame of reasoning, already proposed in the literature on the capillary geochemistry. The consistency of the observations

with the thermodynamic simulation demonstrates the interest to renew our approach of the equilibrium constant when dealing with capillary systems.

Our experiments dealt with cylindrical pores in which cubic crystals grow: touching corners are quite logical. *A posteriori*, we realize that this specific geometry was an enormous chance for the capillary bridges to arise, and for the subsequent process to happen. Nonetheless, any wedge-shape pores, initially present or resulting from a precipitation event, could enable the capillarization and its mechanical traction on the host. An important observation is the ability of these tiny capillary liquid bridges to fossilize while retaining the capillarity state. The NaCl solid bridges appear able to make the in-pore capillary traction more or less independent on the further climatic variations, and so to give it a significant time scale.

We target to connect the studied process with what might happen in the natural media, because our experiments show a non-expected coupling between geochemistry and geomechanics possibly acting inside any non-saturated media. We hypothesize that this heterogeneous stress might be responsible for micro-cracking inside any rock hosting capillary water, especially when the conditions favor the salt precipitation. If this process really takes place in nature, we believe that a re-interpretation of known field data may suffice to confirm the proposition.

We can conclude unambiguously that precipitation of soluble salts in pores changes drastically the capabilities of evolution of the pore system depending on the local conditions, when the in-pore filling is associated with the pore wall cracking. Interestingly, this effect is related to the global permeability of a thin pores rock, but also to the compaction and global firmness of a granular soils, or still to the salt damage in industrial desalination processes or inside the building stones. Finally, the present experimental results offer a new framework of analysis of the global geochemistry-geomechanics coupling processes.

Acknowledgements — E. Tinseau and S. Bassot, of the DEI/SARG/LR2S laboratory of the IRSN, are warmly thanked for their guidance and assistance throughout the experiments. A. Baronnet (CRMC2 lab., CNRS, Marseille) is also gratefully acknowledged for the idea of

cyclohexane rinsing. P. Mirwald and E. Oelkers are greatly acknowledged for their help in improving a first version of this manuscript. Two anonymous reviewers also contributed to improve the manuscript, as well as H. Raimbourg (ISTO, Orleans University) who helped us with the mechanical side of the paper.

REFERENCES

[1] Gerard F., Ranger J., Ménétrier C., and Bonnaud P. (2003) Chem. Geol. 202, 443-460.

[2] Richards P.L. and Kump L.R. (2003) Geochim. Cosmochim. Acta 67(20), 3803-3815.

[3] Mercury L. and Tardy Y. (1997a) C. R. Acad. Sci. Paris 324, 11, 863-873.

[4] Mercury L. and Tardy Y. (1997b) C. R. Acad. Sci. Paris 325, 12, 947-954.

[5] Mercury L. and Tardy Y. (2001) Geochim.Cosmochim. Acta 65, 20, 3391-3408.

[6] Zilberbrand M. (1997) J. Colloid Interf. Sci. 192, 471–474.

[7] Zilberbrand M. (1999) Aquatic Geochem. 5, 195-206.

[8] Mercury L., Azaroual M., Zeyen H., and Tardy Y. (2003) Geochim. Cosmochim. Acta 67, 1769–1785.

[9] Mercury L., Pinti D. L., and Zeyen H. (2004) Earth & Planetary Sci. Lett. 223, 147–161.

[10] Lassin A., Azaroual M., and Mercury L. (2005) Geochim.Cosmochim. Acta 69, 22, 5187-5201.

[11] Mullins C.E. and Panayiotopoulos K.P. (1984) J. Soil Sci. 35, 459-468.

[12] Fredlund D.G. and Rahardjo H. (1993) Soil mechanics for unsaturated soils. J. Wiley & Sons, 517 p.

[13] Mosadegghi, M.R., Hajabbasi M.A., and Khademi H. (2006) Geoderma 134, 160-170.

[14] Hasley T.C. and Levine A.J. (1998) Phys. Rev. Lett. 80(14), 3141-3144.

[15] Fraysse N., Tomé H., and Petit L. (1999) Eur. Phys. J. B, 11(4):615–619.

[16] Scherer G.W. (1990) J. Am. Ceram. Soc. 73(1), 3-14.

[17] Smith D.M., Scherer G.W., and Anderson J.M. (1995) J. Non-Cryst. Solids 188, 191-206.

[18] Tas N.R., Mela P., Kramer T., Berenschot J.W., and van den Berg A. (2003) Nano Lett. 3(11), 1537-1540.

[19] Tas N.R., Escalante M., van Honschoten J.W., Jansen H.V., and Elwenspoek M. (2010) Langmuir 26(3), 1473-1476.

[20] Wellman H.W. and Wilson A.T. (1965) Science 205, 1097-1098.

[21] Kwaad F.J.P.M. (1970) Fysisch Geograph. Bodemkundig Lab. 16, 67-80.

[22] Goudie A.S. and Day M.J. (1980) Phys. Geograph. 1, 126-137.

[23] Mottershead D.N. (1989) Earth Surf. Process. Landforms 14, 383-398.

[24] Warke P.A. and Smith B.J. (2000) Earth Surf. Process. Landforms 25, 1333-1342.

[25] Cahn J.W. (1980) Acta Metall. 28, 1333-1338.

[26] Sanfeld A. and Steinchen A. (2000) Surf. Science 463, 157-173.

[27] Sperling C.H.B. and Cooke R.U. (1985) Earth Surf. Process. Landforms 10, 541-555.

[28] Goudie A.S. (1993) Earth. Surf. Process. Landforms 18, 369-376.

[29] Goudie A.S. and Viles H.A. (1997) Salt weathering hazards. Wiley intersciences. 256 p.

[30] Rodriguez-Navarro C. and Doehne E. (1999) Earth Surf. Process. Landforms 24, 191-209.

[31] Flatt R.J. (2002) J. Cryst. Growth 242, 435-454.

[32] Scherer G.W. (2004) Cement Concrete Res. 34, 1613-1624.

[33] Steiger M. and Asmussen S. (2008) Geochim. Cosmochim. Acta 72, 4291-4306.

[34] Sunagawa I. (1981) Bull. Mineral. 104, 81-87.

[35] Adamson A.W. and Gast A.P. (1997) Physical chemistry of surfaces. J. Wiley & Sons, New York, 6th ed., 808p.

[36] Pitzer K.S. (1991) Activity coefficients in electrolyte solutions. 2nd edition (ed. CRC Press), 542 pp.

[37] Leroy P., Lassin A., and Azaroual M. (2010) Geochim. Cosmochim. Acta (in press, available on the GCA website).

[38] Carstens H. (1986) J. Sedim.Petrol. 56(2), 252-257.

[39] Valès F., Nguyen Minh D., Gharbui H., and Rejeb A. (2004) Applied Clay Sci. 26, 197-207.

[40] Massmann J., Uehara S.-I., Rejeb A., and Millard A. (2009) Environ. Geol. 57, 1337–1345.

[41] Matray J.-M., Parneix J.-C., Tinseau E., Prêt D., and Mayor J.-C. (2007) Clays in Natural & engineered barriers for radioactive waste confinement. Book of abstracts. September 17-18, Lille, France, pp. 445-446.